THE JOURNAL OF PHYSICAL CHEMISTRY C

Article

pubs.acs.org/JPCC

Phosphonic Acid and Lithium Salt as Effective *p*-Dopants to Oxidize Spiro-OMeTAD for Mesoscopic Sb_2S_3 Solar Cells

Chih-Chun Chung, Ting-Wei Tsai, Hui-Ping Wu, and Eric Wei-Guang Diau*

Department of Applied Chemistry and Institute of Molecular Science, National Chiao Tung University, No. 1001, Ta-Hsueh Rd., Hsinchu 30010, Taiwan

Supporting Information

ABSTRACT: 1-Decyl phosphonic acid (DPA) proved an effective *p*-doping additive to oxidize spiro-OMeTAD as a hole-transporting material (HTM) for nanostructured Sb_2S_3 extremely thin absorber (ETA) solar cells. DPA had the effect of enhancing the hole conductivities of spiro-OMeTAD in the presence of lithium bis(trifluoromethyl- sulfonyl)-imide (LiTFSI) to significantly improve the device performance. Transient photoelectric measurements and electrochemical impedance spectra of devices fabricated with varied additive conditions provided information about the charge- transport and recombination kinetics and hole conductivities for Sb_2S_3 devices with additives DPA and LiTFSI that exhibited superior performance. Thirty-five identical devices were fabricated to show the excellent reproducibility and long-term stability in air; the best Sb_2S_3 ETA device attained efficiency of power conversion 6.0%, which is twice that of a device using other typical additives (LiTFSI and 4-*tert*-butyl-pyridine) for spiro-OMeTAD serving as HTM.

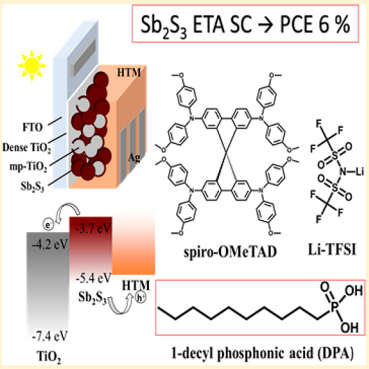

INTRODUCTION

Extremely thin absorber (ETA) solar cells were developed as a promising emerging photovoltaic (PV) technology for next-generation solar cells[1,2] based on a concept similar to solid-state dye-sensitized solar cells (DSSC)[3] and perovskite solar cells (PSC).[4] Instead of organic dyes in a DSSC system, the ETA-sensitized solar cells use purely inorganic semiconducting materials such as chalcogenides[1] to serve as the light-harvesting layer in a thin configuration. Among these chalcogenide candidates, antimony sulfide (Sb_2S_3) is an effective ETA because it absorbs photons in a broad spectral range up to 750 nm with excellent absorption coefficient ($\alpha = 1.8 \times 10^5$ cm^{-1} at 450 nm).[5] Moreover, these mesoscopic ETA devices can be fabricated using a cheap solution-based process such as chemical-bath deposition (CBD)[6] and succeeding ion-layer adsorption and reaction (SILAR)[7] methods with a thin Sb_2S_3 layer deposited on the surface of nanocrystalline TiO_2 that shows great stability in air. Hole-transporting materials (HTM)[6,8−22] of various types were thus reported for Sb_2S_3 ETA solar cells; the best device performance used a conducting polymer (PCPDTBT) to attain an efficiency of power conversion (PCE) exceeding 6%.[16−18]

In contrast, Sb_2S_3 ETA solar cells fabricated with 2,2′,7,7′-tetrakis(*N*,*N*-di-*p*-methoxyphenyl-amine)-9,9′-spirobifluorene (spiro-OMeTAD) as HTM attained only 3.1% with a poor fill factor under one-sun irradiation,[11] which is inconsistent with solid-state solar cells of other types such as DSSC and PSC using spiro-OMeTAD as HTM.[23−25] As a hole conductor, the pristine spiro-OMeTAD is well-known to suffer from poor conductivity, but the conductivity improves significantly on chemical doping with appropriate *p*-type dopants.[26,27] Lithium bis(trifluoromethyl-sulfonyl)-imide (LiTFSI) has been reported to enhance the conductivity and hole mobility in spiro-OMeTAD because the ionic species in the matrix smooth the potential landscape and increase the intramolecular charge transfer.[26] A LiTFSI additive also causes a down-shift of the conduction-band (CB) potential of TiO_2, which has two effects on device performance: (1) enhanced electron injection from the LUMO of the light absorber to the CB of TiO_2 so as to increase the short-circuit photocurrent density (J_{SC})[28,29] and (2) lowered CB of TiO_2 so as to decrease the open-circuit voltage (V_{OC}).[30,31] To compensate the decrease of V_{OC}, 4-tert-butylpyridine (tBP) became another additive in spiro-OMeTAD.[32] Doping with LiTFSI in spiro-OMeTAD was also reported to depend strongly on the ambient oxygen condition or illumination,[30,33,34] which deteriorated the long-term stability and reproducibility of the devices.

Cobalt complexes and superacid H-TFSI have been used as effective *p*-dopants for the oxidation of spiro-OMeTAD to improve the conductivity of the HTM for an enhanced performance of a solid-state DSSC.[27,35] Li et al. reported that phosphoric acid (H_3PO_4) serves as an oxidation catalyst to enhance the conductivity of spiro-OMeTAD for PSC to attain a remarkable device performance.[36] Here we show that 1-decyl phosphonic acid (DPA) combines with LiTFSI to oxidize spiro-OMeTAD effectively to improve the device performance for Sb_2S_3 ETA solar cells. DPA and LiTFSI additives together can be treated as a "protonation generator", as reported for *p*-doping in organic semiconductors to decrease the charge-transport resistance at a photoactive junction.[37−41] We observed the formation of spiro-OMeTAD cations as a function

Received: August 10, 2017
Published: August 11, 2017

DOI: 10.1021/acs.jpcc.7b07958
J. Phys. Chem. C 2017, 121, 18472−18479

of concentration of DPA in the presence of LiTFSI. Concentrations LiTFSI (40 mM) and DPA (50 mM) optimized the device performance; 35 identical devices were fabricated to show the excellent reproducibility for the PCE distribution spanning a narrow range. The best device performance of the Sb_2S_3 ETA solar cell attained PCE 6.0%, which is almost twice that of devices made of spiro-OMeTAD as HTM with other additives,[11] and comparable to those made with conducting polymers as HTM.[17,18] Transient photoelectric measurements and electrochemical impedance spectra provided data about the charge-transport kinetics and hole conductivities in relation to the device performances for Sb_2S_3 cells under varied additive conditions. To the best of our knowledge, this report is the first of the use of DPA and LiTFSI as *p*-dopants to attain effective oxidation of spiro-OMeTAD for highly efficient Sb_2S_3 ETA solar cells with satisfactory long-term stability.

RESULTS AND DISCUSSION

The Sb_2S_3 ETA solar cells were fabricated according to the device configuration FTO/c-TiO_2/mp-TiO_2/Sb_2S_3/spiro-OMeTAD/Ag, as shown in Figure 1a; the device fabrication

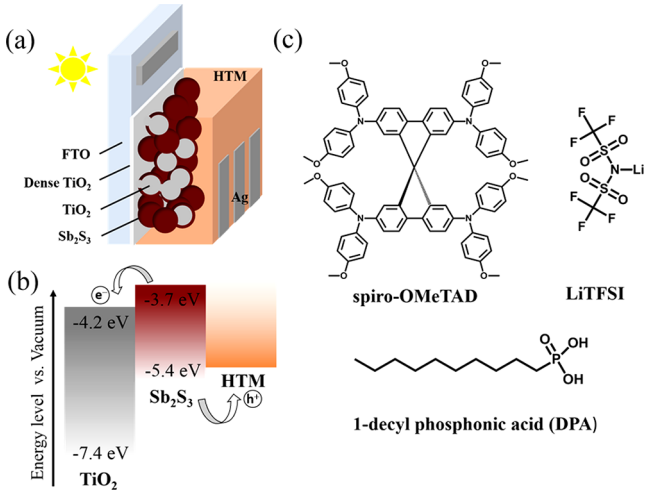

Figure 1. (a) Device structure of a Sb_2S_3 absorber (ETA) in a sensitized solar cell, (b) energy-level diagram for each component of the device with the energy levels reported elsewhere,[1] and (c) chemical structures of the corresponding HTM and additive materials.

is shown in Figure S1. A compact TiO_2 layer (c-TiO_2, thickness ~ 60 nm) was deposited on a FTO substrate with a thermal spray method followed by deposition of a mesoporous TiO_2 layer (mp-TiO_2, thickness ~ 900 nm) using screen printing. Sb_2S_3 light absorber in a thin layer was deposited on the mp-TiO_2 layer according to the CBD method reported elsewhere;[13,17] a layer of spiro-OMeTAD (thickness ~220 nm) to serve as HTM was then spin-coated on top of the mp-TiO_2/Sb_2S_3 layer followed by coating with Ag (thickness ~80 nm) as a back contact layer to complete the device fabrication. The corresponding energy levels of the three major components, mp-TiO_2/Sb_2S_3/spiro-OMeTAD, are shown in Figure 1b, indicating an effective match of energy levels for electron and hole propagation.[1] The chemical structures of spiro-OMeTAD and its two *p*-doping additives (LiTFSI and DPA) are shown in Figure 1c.

Figure S2 (panels a and b) shows top-view SEM images of the mp-TiO_2 layer without and with covering the thin Sb_2S_3 absorber layer, respectively. Figures S2c shows at high resolution a TEM image of the mp-TiO_2 layer covered with Sb_2S_3; the enlarged TEM image of the red square area is shown in Figure S2d. The well-defined nanocrystalline nature of mp-TiO_2 is observable in Figure S2d; the yellow dotted curve shows the boundary of the TiO_2/Sb_2S_3 interface. The thickness of the Sb_2S_3 absorber layer was estimated to be ~10 nm.

Traditional Sb_2S_3-sensitized solid-state solar cells using spiro-OMeTAD as HTM gave PCE only 3.1% under one-sun irradiation.[11] As pristine spiro-OMeTAD is well-known to suffer from poor conductivity, chemical *p*-doping additives such as tin chloride,[43] H-TFSI,[35] and cobalt complexes[27] were utilized as additives to improve the hole-conducting ability of a solid-state DSSC using spiro-OMeTAD as HTM. These additives led to oxidation of spiro-OMeTAD; the corresponding ionic spectral feature of the hole conductor was unambiguously observed.[27,35,43] Among other *p*-type semiconductors that serve as HTM for Sb_2S_3 ETA solar cells, CuSCN was employed as a hole conductor for all inorganic ETA solar cells.[6,8,44] In that case, varied *p*-dopants were examined with a surface treatment of LiSCN or KSCN before or after the deposition of CuSCN. These interfacial treatments induced phase changes of CuSCN and had the effect of facilitating the diffusion of K^+ ions into the CuSCN layer as a *p*-dopant to align the energy levels between Sb_2S_3 and the HTM layer.[44] Moreover, K-doping can passivate the surface trap states of CuSCN and result in a decreased series resistance of HTM and enhanced device performance. As pointed out elsewhere,[9] the key factor to increase the efficiency of Sb_2S_3 ETA solar cells is to enhance the hole-transporting property, in particular to improve the hole mobility for hole conductors of varied types applied in these ETA cells.

In our approach, we used DPA to oxidize spiro-OMeTAD in the presence of LiTFSI; the corresponding absorption spectra with DPA at varied proportions are shown in Figure 2 (panels a–c). The absorption with maximum at 388 nm is assigned to neutral spiro-OMeTAD. Upon increasing the concentration of DPA, the observed enhanced absorption for the 520 nm bands (Figure 2b) and for the 1600 nm bands (Figure 2c) is clear evidence for oxidation of spiro-OMeTAD via DPA and LiTFSI. The *J*–*V* curves and IPCE spectra of the Sb_2S_3-sensitized ETA devices with DPA additive at varied concentrations and a fixed amount of LiTFSI are shown in Figure S3 (panels a and b, respectively); the corresponding photovoltaic parameters are summarized in Table S1. The reference cell is the Sb_2S_3 device with only LiTFSI (20 mM) but no DPA additive; this cell attained a PCE of 3.4%. When DPA was added at varied concentration, the device performance increased until [DPA] = 50 mM, for which the PCE increased to 5.3%. We observed that J_{SC}, V_{OC}, FF, and PCE were all enhanced on increasing the concentration of DPA from 0 to 50 mM, but the performance decreased on further increasing DPA to 100 mM (PCE = 4.5%). The enhanced photovoltaic performance might be attributed to the increased conductivity of spiro-OMeTAD with DPA and LiTFSI as *p*-dopants to generate more oxidized HTM for a superior charge separation. When [DPA] was increased to 100 mM, the excess oxidized spiro-OMeTAD species might induce charge recombination with electrons generated by photoinduced Sb_2S_3 so that both J_{SC} and V_{OC} were smaller with DPA at 100 mM than at 50 mM.

To investigate the effect of the LiTFSI additive in the spiro-OMeTAD solution, we measured *J*–*V* curves with LiTFSI salt at varied concentration; this well-known additive effectively

DOI: 10.1021/acs.jpcc.7b07958
J. Phys. Chem. C 2017, 121, 18472–18479

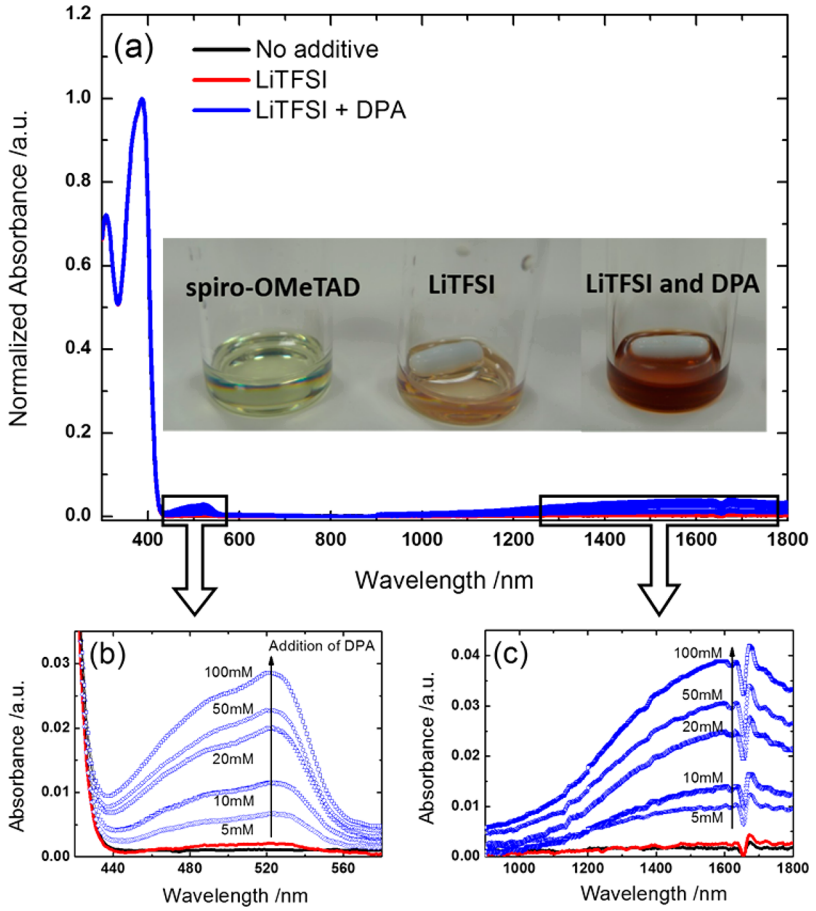

Figure 2. (a) Absorption spectra of spiro-OMeTAD solutions from 300 to 1800 nm for varied additive conditions (black: no additive; red: LiTFSI; blue: LiTFSI and DPA in varied concentrations). (b) Extension of spectra in a range from 420 to 580 nm. (c) Extension of spectra in the range from 900 to 1800 nm. The concentration of spiro-OMeTAD is 0.145 M and that of LiTFSI is 20 mM.

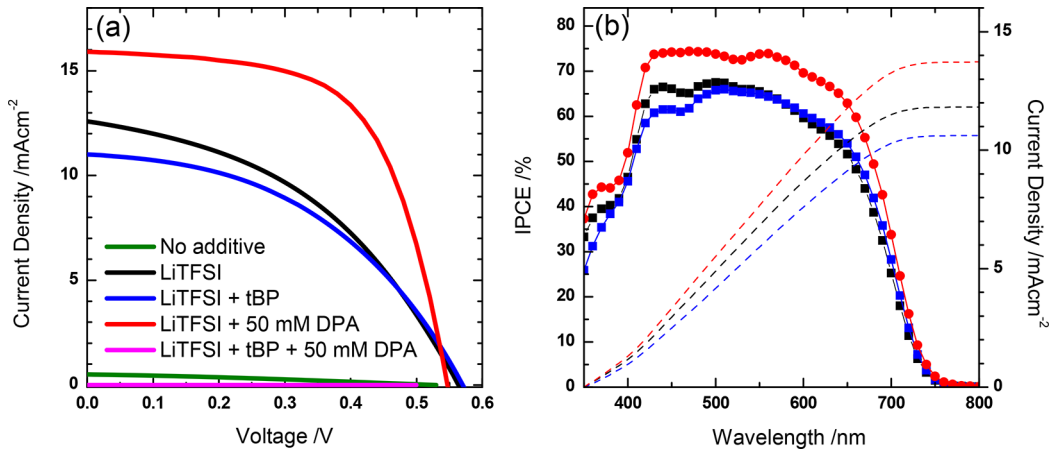

Figure 3. (a) $J-V$ characteristics under AM-1.5G simulated illumination and (b) the corresponding IPCE spectra of Sb_2S_3 ETA solar cells with various additive conditions in spiro-OMeTAD as indicated. The concentrations are spiro-OMeTAD, 0.145 M; LiTFSI, 40 mM; tBP, 200 mM; and DPA, 50 mM.

enhances the conductivity of spiro-OMeTAD. The corresponding $J-V$ curves appear in Figure S4; the photovoltaic parameters are summarized in Table S2. The conductivity of pristine spiro-OMeTAD was poor, which caused the device to show almost no performance (PCE = 0.1%); with DPA additive (50 mM) the device performance improved only slightly (from 0.1% to 0.7%), but when both LiTFSI and DPA were added into spiro-OMeTAD, we observed a significantly enhanced device performance, as the results in Table S2 show. For DPA fixed at 50 mM, increasing concentration of LiTFSI increased J_{SC} until [LiTFSI] = 40 mM; J_{SC} then decreased continuously from 60 mM to 120 mM. These results are explained with excess Li^+ ions intercalating on the surface of TiO_2 for LiTFSI at large concentrations, which induces more trap states to impede the electrons generated from Sb_2S_3 from injecting into TiO_2.[30,45] Furthermore, a systematic decrease of V_{OC} was

DOI: 10.1021/acs.jpcc.7b07958
J. Phys. Chem. C 2017, 121, 18472−18479

observed upon increasing the concentrations of LiTFSI because of downward shifts of the conduction-band potentials of TiO_2 with intercalating Li^+.[30,46] The optimized concentrations for the Sb_2S_3 devices were hence determined to be LiTFSI 40 mM and DPA 50 mM. A side-view SEM image of the best performing Sb_2S_3 device is shown in Figure S5.

We have demonstrated that DPA plays an important role in oxidizing spiro- OMeTAD to improve the conductivity of HTM in the presence of the LiTFSI salt. To improve V_{OC} of the device, we added 4-*tert*-butylpyridine (tBP) in HTM as in the case of other solid-state solar cells,[11] but we found that tBP has a negative effect on device performance as an additive together with DPA. Figure 3 (panels a and b) show the $J-V$ characteristics and IPCE spectra, respectively, of the Sb_2S_3 ETA solar cells fabricated with various additive combinations in spiro-OMeTAD; corresponding photovoltaic parameters are listed in Table 1. The tBP additive had the effect to increase

Table 1. Photovoltaic Parameters of Sb_2S_3 ETA Solar Cells Based on Spiro-OMeTAD Containing Various Additives under Simulated AM-1.5G Illumination (Power Density 100 mW cm^{-2}) with Active Area 0.09 cm^2

spiro-OMeTAD[a]	J_{SC} (mA cm^{-2})	V_{OC} (mV)	FF	PCE (%)
no additive	0.51	529	0.305	0.1
LiTFSI	12.60	564	0.425	3.0
LiTFSI + tBP	11.01	571	0.447	2.8
LiTFSI + DPA	15.91	548	0.613	5.4
LiTFSI + tBP + DPA	0.001	473	0.261	0.0

[a]The concentrations are spiro-OMeTAD, 0.145 M; LiTFSI, 40 mM; tBP, 200 mM; and DPA, 50 mM.

V_{OC} slightly from 564 (LiTFSI) to 571 mV (LiTFSI + tBP), but it caused J_{SC} to decrease significantly because the basic property of tBP might induce corrosion of the Sb_2S_3 absorber layer. As discussed above, adding DPA and LiTFSI enhanced J_{SC} and FF significantly and gave PCE 5.4%. In contrast, when tBP was added with LiTFSI and DPA, we found almost no performance of that device. In this case, the spiro-OMeTAD solution exhibited a viscous gel property due to the neutralization of tBP (a base) and DPA (an acid), which accounts for the poor device performance with these three additives together in spriro-OMeTAD. The best performing cell remains the LiTFSI + DPA device, for which the IPCE spectra exhibited a photocurrent response over 75% in the visible spectral region to account for J_{SC} (15.9 mA cm^{-2}), superior to that of other Sb_2S_3 devices.

To understand the influence of LiTFSI on device performance, we performed transient photoelectric measurements[42] for the devices at three concentrations (40, 60, and 120 mM) in the presence of DPA (fixed at 50 mM) using the charge-extraction (CE), transient photovoltage-decay (TVD), and transient photocurrent-decay (TCD) methods; the results appear in Figure S6 (panels a–c, respectively). For the CE measurements, Figure S6a shows plots of V_{OC} versus extracted charge density (N_e) at seven bias light intensities; the results indicate that V_{OC} values of devices obtained with LiTFSI at varied concentrations showed a trend with V_{OC} (40 mM) > V_{OC} (60 mM) > V_{OC} (120 mM), compared at the same N_e level, confirming that more Li^+ ions intercalated on the surface of TiO_2 lowered the Fermi level of the conduction band of TiO_2. For the TVD, we measured the charge-recombination time coefficient (τ_{rec}) at seven bias light intensities via transients induced with a probe LED pulse at an open-circuit condition. Figure S6b shows plots of τ_{rec} versus N_e for the devices made with LiTFSI at three concentrations; the device at 120 mM had the longest charge recombination lifetime, attributed to a retarded charge recombination with a possible screening of the Coulomb attraction between holes in the spiro-OMeTAD and electrons in the TiO_2.[30,47,48] Figure S6c shows plots of the charge-collection time coefficient (τ_c) versus J_{SC} under a short-circuit condition at seven bias light intensities. The trend on increasing τ_c with increasing LiTFSI concentration is consistent with a decreasing trend of J_{SC} shown in Table S2 because increasing the surface traps by Li^+ intercalation with increased LiTFSI concentration increased the detrapping rates on the TiO_2 surface, leading to a poor charge collection.[30,49]

Photoelectric transient measurements enabled a comparison with other devices for devices made of LiTFSI with those made of LiTFSI + tBP and LiTFSI + DPA; the results appear in Figure 4. Plots of V_{OC} versus N_e and τ_{rec} versus N_e are shown in Figure 4a. With the LITFSI additive as a reference, the addition of tBP or DPA down-shifted the CB level of TiO_2, but both tBP and DPA additives had the effect of retarding the charge recombination, leading to a trend for V_{OC} with order LiTFSI + tBP (571 mV) > LiTFSI only (564 mV) > LiTFSI + DPA (548 mV); their discrepancies are not very significant. In contrast, Figure 4b shows a trend for the charge-collection coefficient with order τ_c (LiTFSI + DPA) < τ_c (LiTFSI) < τ_c (LiTFSI + tBP), indicating that the conductivity of spiro-OMeTAD might be enhanced with additives LiTFSI and DPA. These results are

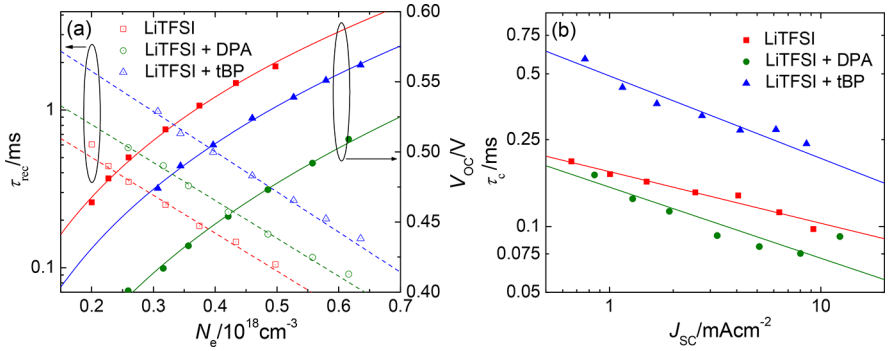

Figure 4. Plots of (a) V_{OC} as a function of extracted charge density (N_e) and charge-recombination time coefficient (τ_{rec}) as a function of N_e at an open-circuit condition and (b) charge-collection time coefficient (τ_c) as a function of J_{SC} at a short-circuit condition for Sb_2S_3 ETA solar cells with varied additive condition as indicated. The concentrations are spiro-OMeTAD, 0.145 M; LiTFSI, 40 mM; tBP, 200 mM; and DPA, 50 mM.

DOI: 10.1021/acs.jpcc.7b07958
J. Phys. Chem. C 2017, 121, 18472–18479

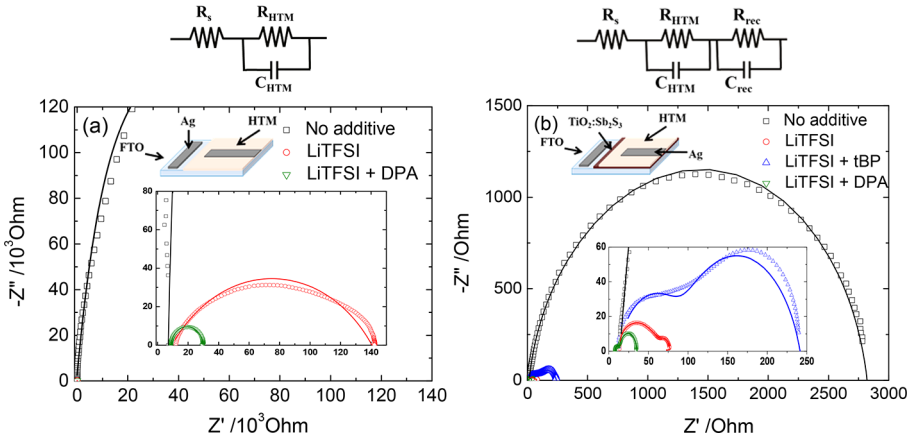

Figure 5. Nyquist plots of (a) devices made of only HTM (spiro-OMeTAD) with varied additives measured in darkness and (b) Sb_2S_3 ETA solar cells with varied additives under one-sun illumination and open-circuit conditions. The equivalent-circuit models for fitting the EIS data (Z-view software) are shown on top of the figures. The insets show enlarged plots.

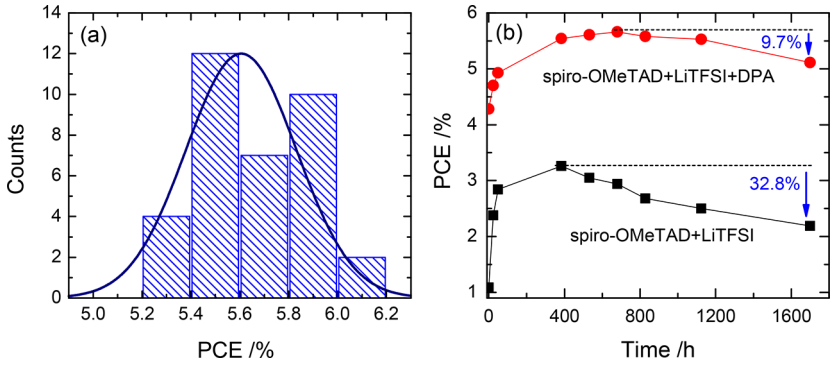

Figure 6. (a) Histogram of PCE of Sb_2S_3 ETA solar cells (LiTFSI + DPA) with 35 devices fabricated under the same conditions. (b) Stability characteristics of Sb_2S_3 ETA solar cells with and without DPA additive. Data are presented for the ambient atmosphere: 20 °C, relative humidity of 50%, and no encapsulation.

consistent with the trend of J_{SC}: LiTFSI + DPA (15.91 mA cm^{-2}) > LiTFSI only (12.60 mA cm^{-2}) > LiTFSI + tBP (11.01 mA cm^{-2}). We hence expect that Sb_2S_3 ETA solar cells with the LiTFSI + DPA additive would increase the charge carriers inside spiro-OMeTAD through the effective oxidation of the HTM that assists charge collection. Although V_{OC} obtained for the LiTFSI + DPA device was slightly less than for the others, the much enhanced J_{SC} value made this device show a device performance (PCE 5.4%) greater than that of other devices. The oxidation of spiro-OMeTAD in the presence of DPA and LiTFSI thus plays an important role to improve the conductivity of the HTM and the overall device performance.

Electrochemical impedance spectra (EIS) were recorded in the frequency range from 100 mHz to 4 MHz for two device configurations. Figure 5 (panels a and b) shows Nyquist plots of devices made of only spiro-OMeTAD and Sb_2S_3 ETA solar cells with varied additives; the fitted impedance parameters according to the equivalent circuit models shown on top of the figures are summarized in Table S3. In Figure 5a, the Nyquist plots show only one arc feature with R_{HTM} values corresponding to the conductivities of the HTM (pristine spiro-OMeTAD without additive), HTM + LiTFSI, and HTM + LiTFSI + DPA. The EIS results show that R_{HTM} of pristine spiro-OMeTAD was large without additives; the value of R_{HTM} decreased significantly in the presence of LiTFSI. With LiTFSI and DPA added together to spiro-OMeTAD, the value of R_{HTM} further decreased, indicating that additives DPA + LiTFSI have the effect of decreasing the charge-transfer resistance in the HTM layer to account for J_{SC} of this device being greater than the others. FF of the devices also showed a systematic trend: DPA + LiTFSI (0.613) > LiTFSI (0.425) > no additive (0.305), which is well-explained with the EIS results for the small impedance of the DPA + LiTFSI device being due to the enhanced conductivity of HTM in the presence of the two additives.

For the EIS of the complete Sb_2S_3 ETA devices shown in Figure 5b, we observed that data show a two-arc feature corresponding to two sets of RC elements in the equivalent circuit: the arc at large frequency is assigned to the contribution of HTM, whereas the other arc reflects the contribution of charge transfer in the TiO_2/Sb_2S_3/HTM interfaces. We hence assign impedance elements R_{HTM} and R_{rec} to correspond to the low- and high-frequency arcs, respectively. The R_{HTM} values in Figure 5b show the same trend as those in Figure 5a but with much smaller values because of the varied experimental conditions: the devices with HTM only were measured in darkness (Figure 5a), whereas the complete Sb_2S_3 ETA devices were measured under one-sun illumination (Figure 5b). The Sb_2S_3 device with additives LiTSFI and DPA gave the least R_{HTM} value among all devices, confirming the results measured with HTM-only devices. In the low-frequency range, the arc with characteristic resistance R_{rec} arose from charge recombination between the TiO_2 and the HTM layers when the impedances were measured under an open-circuit condition.

DOI: 10.1021/acs.jpcc.7b07958
J. Phys. Chem. C 2017, 121, 18472−18479

Because of the varied effect of the HTM additives on charge recombination, we observed R_{rec} values with the trend no additive > LiTFSI + tBP > LiTFSI + DPA > LiTFSI. The device without additive exhibited the largest R_{rec} because the poor conductivity of pristine spiro-OMeTAD became a bottleneck for the slow charge recombination to occur. For the other devices, the trend of R_{rec} is consistent with the trend of the TVD results shown in Figure 4a. In accordance with our EIS results, the LiTFSI additive can improve the conductivity to some extent but it affects the charge recombination more significantly. Adding tBP together with LiTFSI is a typical treatment for solid-state DSSC[3] and perovskite solar cells,[4] but, for the Sb_2S_3 ETA cells, LiTFSI + tBP retarded the charge recombination and concurrently enhanced R_{HTM} to decrease the conductivity of the hole conductor. Adding DPA with LiTFSI had an effect to decrease R_{HTM} significantly, to enhance the conductivity of the HTM. Although the effect to retard charge recombination for the LiTFSI + DPA device was moderate, the superior conductivity of the HTM had an effect to improve both J_{SC} and FF, where the result differs from that of Li et al.[36] who found that phosphoric acid with LiTFSI had an effect of improving V_{OC} and FF for perovskite solar cells.

The performances of the LiTFSI + DPA devices were optimized on tuning the thickness of the c-TiO_2 compact layer; a thin compact layer (~20 nm) further enhanced both J_{SC} and FF and thus gave a better overall device performance. As a result, thirty-five identical such devices were fabricated at the same experimental conditions to show the reproducibility of the performance; the photovoltaic data are shown in Table S4; the corresponding PCE histogram in Figure 6a indicates a narrow distribution of photovoltaic performance, spanning the range of 5.2−6.0%, with an average PCE of 5.6 ± 0.2. The best Sb_2S_3 ETA device displayed J_{SC} = 17.05 mA cm^{-2}, V_{OC} = 553 mV, FF = 0.636, and PCE = 6.0%, similar to those reported using conducting polymers (e.g., P3HT and PCPDTBT) as HTM.[17,18]

It is an important issue to demonstrate the stability of Sb_2S_3 ETA solar cells, for which the device performance was recorded as a function of storage period in ambient atmospheric conditions without encapsulation. As Figure 6b shows, the device performance of Sb_2S_3 ETA solar cell with additives LiTFSI and DPA deteriorated only 10% from the highest value over 1700 h of storage, whereas the device performance with only additive LiTFSI (no DPA) deteriorated for over 30%. The hydrophobicity of the HTM layer on adding a long-chain acid such as DPA is expected to be a key factor for superior performance stability without added DPA. We hence show here the excellent long-term stability with great device performance for Sb_2S_3 ETA solar cells using spiro-OMeTAD as HTM, for which the additive DPA plays an important role to form a stable device against deterioration of performance in atmospheric moisture conditions.

CONCLUSION

Spiro-OMeTAD is a well-known hole-transporting material (HTM) that is applied widely in solid-state dye-sensitized solar cells and perovskite solar cells to obtain device performance superior to that using other HTM.[1,4] When spiro-OMeTAD was applied to Sb_2S_3 ETA solar cells with traditional *p*-doping additives (LiTFSI, tBP, and so forth), the device performance was much poorer than for those using conducting polymers as HTM.[13,16−18] Here we introduced an acid additive, 1-decyl phosphonic acid (DPA), as an effective *p*-dopant to oxidize spiro-OMeTAD in the presence of LiTFSI to enhance the conductivity of the HTM, to improve the device performance. The extent of oxidation of spiro-OMeTAD increased systematically with increasing concentration of DPA and fixed concentration of LiTFSI probed with the absorption spectra 300−1800 nm. DPA alone cannot oxidize spiro-OMeTAD, but the acid catalyzes the oxidation of spiro-OMeTAD in the presence of LiTFSI. The amounts of DPA and LiTFSI were varied separately to find the combination of optimum device performance for Sb_2S_3 ETA solar cells. Both transient photoelectric measurements and electrochemical impedance spectra were utilized to characterize the charge transport and recombination kinetics and hole conductivities of the devices to understand the mechanism of oxidation of the varied *p*-doping additives (no additive, LiTFSI, LiTFSI + tBP, LiTFSI + DPA, and LiTFSI + DPA + tBP) relative to the corresponding device performance. The addition of tBP with LiTFSI slightly improved V_{OC} of the device, but the decreased J_{SC} led to a performance poorer than those of LiTFSI and LiTFSI + DPA devices. Adding tBP with LiTFSI and DPA together resulted in almost no efficiency because of the acid−base reaction between DPA and tBP additives. The LiTFSI + DPA device exhibited the best performance with significantly improved J_{SC} and FF with respect to those without added DPA. Thirty-five LiTFSI + DPA devices were fabricated under the same experimental conditions; the reproducibility of the performance was confirmed with the best device showing J_{SC} = 17.05 mA cm^{-2}, V_{OC} = 553 mV, FF = 0.636, and PCE = 6.0%, which is comparable to those reported using conducting polymers as HTM.[17,18] The LiTFSI + DPA device also exhibited great long-term stability in ambient air conditions due to the increased hydrophobicity of the HTM layer with a long-chain acid such as DPA as an additive. The present results thus provide a new perspective for this approach applicable for solar cells of other types such as solid-state DSSC and PSC for further improvement of their device performance.

EXPERIMENTS

Devices Fabrication. TiO_2 (layer thickness ~60 nm) was deposited on FTO glass (TEC7, Hartford) via spray pyrolysis of titanium diisopropoxide bis(acetylacetonate) (TAA, 0.5 M) precursor in ethanol solution. To achieve the device optimization and to decrease efficiently the series resistance, a thin TiO_2 under layer (~20 nm) was deposited from a dilute TAA solution (0.05 M in ethanol), followed by a post treatment of $TiCl_4$ (70 °C, 30 min) and annealed at 500 °C for 20 min. The mesoporous TiO_2 layers (thickness 1 μm) were prepared on screen-printing of TiO_2 paste (P25, Degussa) and annealed at 500 °C for 30 min, followed by post treatment with $TiCl_4$ (0.01 M) for 10 min at 70 °C, and annealing at 500 °C for 30 min to improve the interconnection of the TiO_2 particles. The Sb_2S_3 sensitizer was synthesized on the surface of mesoporous TiO_2 film by means of a chemical-bath deposition (CBD). $SbCl_3$ (1.3 g, Alfa Aesar) was dissolved in propanone (5 mL); $Na_2S_2O_3$ solution (50 mL, 1M, Alfa Aesar) and deionized water (145 mL) were kept at a temperature below 4 °C in a refrigerator. The cold $SbCl_3$, $Na_2S_2O_3$ solutions, and deionized water were mixed to form a nearly clear solution. Substrates were placed vertically in a CBD bath for 3 h at 4−7 °C. The Sb_2S_3-coated TiO_2 films were annealed at ~330 °C for 30 min under an inert atmosphere to form stibnite nanocrystals. Spiro-OMeTAD (0.145M) as hole-transporting material with various dopants or additives (e.g.,

DOI: 10.1021/acs.jpcc.7b07958
J. Phys. Chem. C 2017, 121, 18472−18479

tBP, LiTFSI, and DPA) was spin-coated on TiO_2/Sb_2S_3 films in a glovebox at 2500 rpm for 60 s. Silver (150 nm) was deposited on the HTM layer as a back-contact electrode under high-vacuum condition (10^{-6} Torr).

Characterization. Absorption spectra (350−1800 nm) were recorded (Jasco V-570 spectrophotometer) to observe the signals of oxidized species of spiro-OMeTAD. A field-emission scanning electron microscope (FESEM, SU8010, Hitachi) and a high-resolution transmission electron microscope (HRTEM, JEM-2100, JEOL) were used to investigate the morphology and structure of the samples, respectively. The $J-V$ characteristics of devices were recorded with a digital source meter (Keithley 2400) under one-sun illumination (AM 1.5G, 100 mW cm^{-2}) with a solar simulator (XES-40S1, SAN-E1) and was calibrated with a silicon diode and KG-5 filter. The efficiency of spectra of conversion of incident photons to current (IPCE) was recorded with a system comprising a Xe lamp (A-1010, PTi, 150 W) and a monochromator (PTi). The transient photoelectric measurements were performed according to methods reported elsewhere.[42] To measure charge extraction, we used a white-light LED as a bias source to illuminate the devices under an open-circuit steady condition; the bias light was extinguished simultaneously with the system being switched to the short-circuit condition. The current transient under the latter condition was recorded and converted to a total charge density (N_e/cm^{-3}); the photovoltage and photocurrent transient-decay experiments were recorded on a digital oscilloscope (MSO2014, Tektronix), with signals passing a current preamplifier (SR570, SRS) at a short-circuit condition and a voltage preamplifier (SR560, SRS) at an open-circuit condition, respectively. The electrochemical impedance spectral measurements for devices made of only HTM layers or complete Sb_2S_3 ETA solar cells were recorded over a frequency range of 100 mHz to 4 MHz with ac amplitude 10 mV under one-sun illumination and open-circuit condition. The obtained EIS data were fitted (Z-view software) based on the corresponding equivalent circuit models.

■ ASSOCIATED CONTENT

Supporting Information

The Supporting Information is available free of charge on the ACS Publications website at DOI: 10.1021/acs.jpcc.7b07958.

Solar cell device fabrication, SEM and TEM images, $J-V$ spectra, photovoltaic parameters, side-view SEM image, plots of V_{OC} as a function of charge density, charge recombination lifetime as a function of N_e, and charge collection lifetime, and impedance parameters of HTM only (PDF)

■ AUTHOR INFORMATION

Corresponding Author

*E-mail: diau@mail.nctu.edu.tw.

ORCID

Eric Wei-Guang Diau: 0000-0001-6113-5679

Notes

The authors declare no competing financial interest.

■ ACKNOWLEDGMENTS

We thank Drs. Jae Hui Rhee and Yu-Cheng Chang for their assistance and suggestions on sample preparation and characterizations. Ministry of Science and Technology (MOST) of Taiwan supported this work with contracts MOST105-2119-M-009-011-MY3 and MOST 105-2119-M-009-001.

■ REFERENCES

(1) Rhee, J. H.; Chung, C.-C.; Diau, E. W.-G. A perspective of mesoscopic solar cells based on metal chalcogenide quantum dots and organometal-halide perovskites. *NPG Asia Mater.* **2013**, *5*, e68.

(2) Diau, E. W.-G. Next-Generation Solar Cells and Conversion of Solar Energy. *ACS Energy Lett.* **2017**, *2*, 334−335.

(3) Hagfeldt, A.; Boschloo, G.; Sun, L.; Kloo, L.; Pettersson, H. Dye-Sensitized Solar Cells. *Chem. Rev.* **2010**, *110*, 6595−6663.

(4) Correa-Baena, J. P.; Abate, A.; Saliba, M.; Tress, W.; Jesper Jacobsson, T.; Gratzel, M.; Hagfeldt, A. The rapid evolution of highly efficient perovskite solar cells. *Energy Environ. Sci.* **2017**, *10*, 710−727.

(5) Versavel, M. Y.; Haber, J. A. Structural and optical properties of amorphous and crystalline antimony sulfide thin-films. *Thin Solid Films* **2007**, *515*, 7171−7176.

(6) Itzhaik, Y.; Niitsoo, O.; Page, M.; Hodes, G. Sb_2S_3-Sensitized Nanoporous TiO_2 Solar Cells. *J. Phys. Chem. C* **2009**, *113*, 4254−4256.

(7) Salunkhe, D. B.; Gargote, S. S.; Dubal, D. P.; Kim, W. B.; Sankapal, B. R. Sb_2S_3 nanoparticles through solution chemistry on mesoporous TiO_2 for solar cell application. *Chem. Phys. Lett.* **2012**, *554*, 150−154.

(8) Nezu, S.; Larramona, G.; Choné, C.; Jacob, A.; Delatouche, B.; Péré, D.; Moisan, C. Light Soaking and Gas Effect on Nanocrystalline TiO_2/Sb_2S_3/CuSCN Photovoltaic Cells following Extremely Thin Absorber Concept. *J. Phys. Chem. C* **2010**, *114*, 6854−6859.

(9) Christians, J. A.; Kamat, P. V. Trap and Transfer. Two-Step Hole Injection Across the Sb_2S_3/CuSCN Interface in Solid-State Solar Cells. *ACS Nano* **2013**, *7*, 7967−7974.

(10) Ito, S.; Tsujimoto, K.; Nguyen, D.-C.; Manabe, K.; Nishino, H. Doping Effects in Sb_2S_3 Absorber for Full-Inorganic Printed Solar Cells with 5.7% Conversion Efficiency. *Int. J. Hydrogen Energy* **2013**, *38*, 16749−16754.

(11) Moon, S. J.; Itzhaik, Y.; Yum, J. H.; Zakeeruddin, S. M.; Hodes, G.; Grätzel, M. Sb_2S_3-Based Mesoscopic Solar Cell using an Organic Hole Conductor. *J. Phys. Chem. Lett.* **2010**, *1*, 1524−1527.

(12) Kang, H. W.; Lee, J. W.; Park, N. G. Effect of Double Blocking Layers at TiO_2/Sb_2S_3 and Sb_2S_3/spiro-MeOTAD Interfaces on Photovoltaic Performance. *Faraday Discuss.* **2014**, *176*, 287−299.

(13) Chang, J. A.; Rhee, J. H.; Im, S. H.; Lee, Y. H.; Kim, H.-j.; Seok, S. I.; Nazeeruddin, M. K.; Gratzel, M. High-Performance Nanostructured Inorganic−Organic Heterojunction Solar Cells. *Nano Lett.* **2010**, *10*, 2609−2612.

(14) Fukumoto, T.; Moehl, T.; Niwa, Y.; Nazeeruddin, M. K.; Grätzel, M.; Etgar, L. Effect of Interfacial Engineering in Solid-State Nanostructured Sb_2S_3 Heterojunction Solar Cells. *Adv. Energy Mater.* **2013**, *3*, 29−33.

(15) Huerta-Flores, A. M.; García-Gómez, N. A.; de la Parra-Arciniega, S. M.; Sánchez, E. M. Fabrication and Characterization of a Nanostructured TiO_2/In_2S_3-Sb_2S_3/CuSCN Extremely Thin Absorber (ETA) solar cell. *Semicond. Sci. Technol.* **2016**, *31*, 085011.

(16) Choi, Y. C.; Lee, D. U.; Noh, J. H.; Kim, E. K.; Seok, S. I. Highly Improved Sb_2S_3 Sensitized-Inorganic−Organic Heterojunction Solar Cells and Quantification of Traps by Deep-Level Transient Spectroscopy. *Adv. Funct. Mater.* **2014**, *24*, 3587−3592.

(17) Chang, J. A.; Im, S. H.; Lee, Y. H.; Kim, H. j.; Lim, C. S.; Heo, J. H.; Seok, S. I. Panchromatic Photon-Harvesting by Hole-Conducting Materials in Inorganic−Organic Heterojunction Sensitized-Solar Cell through the Formation of Nanostructured Electron Channels. *Nano Lett.* **2012**, *12*, 1863−1867.

(18) Im, S. H.; Lim, C. S.; Chang, J. A.; Lee, Y. H.; Maiti, N.; Kim, H. J.; Nazeeruddin, M. K.; Grätzel, M.; Seok, S. I. Toward Interaction of Sensitizer and Functional Moieties in Hole-Transporting Materials for Efficient Semiconductor-Sensitized Solar Cells. *Nano Lett.* **2011**, *11*, 4789−4793.

DOI: 10.1021/acs.jpcc.7b07958
J. Phys. Chem. C 2017, 121, 18472−18479

(19) Parize, R.; Katerski, A.; Gromyko, I.; Rapenne, L.; Roussel, H.; Kärber, E.; Appert, E.; Krunks, M.; Consonni, V. ZnO/TiO_2/Sb_2S_3 Core−Shell Nanowire Heterostructure for Extremely Thin Absorber Solar Cells. *J. Phys. Chem. C* **2017**, *121*, 9672−9680.
(20) Kamruzzaman, M.; Chaoping, L.; Yishu, F.; Farid Ul Islam, A. K. M.; Zapien, J. A. Atmospheric annealing effect on TiO_2/Sb_2S_3/P3HT heterojunction hybrid solar cell performance. *RSC Adv.* **2016**, *6*, 99282−99290.
(21) Osorio Mayon, Y.; White, T. P.; Wang, R.; Yang, Z.; Catchpole, K. R. Evaporated and solution deposited planar Sb_2S_3 solar cells: A comparison and its significance. *Phys. Status Solidi A* **2016**, *213*, 108−113.
(22) Godel, K. C.; Choi, Y. C.; Roose, B.; Sadhanala, A.; Snaith, H. J.; Seok, S. I.; Steiner, U.; Pathak, S. K. Efficient Room Temperature Aqueous Sb_2S_3 Synthesis for Inorganic-Organic Sensitized Solar Cells with 5.1% Efficiencies. *Chem. Commun.* **2015**, *51*, 8640−8643.
(23) Saliba, M.; Matsui, T.; Domanski, K.; Seo, J. Y.; Ummadisingu, A.; Zakeeruddin, S. M.; Correa-Baena, J. P.; Tress, W. R.; Abate, A.; Hagfeldt, A.; Gratzel, M. Incorporation of rubidium cations into perovskite solar cells improves photovoltaic performance. *Science* **2016**, *354*, 206−209.
(24) Ahn, N.; Son, D. Y.; Jang, I. H.; Kang, S. M.; Choi, M.; Park, N. G. Highly Reproducible Perovskite Solar Cells with Average Efficiency of 18.3% and Best Efficiency of 19.7% Fabricated via Lewis Base Adduct of Lead(II) Iodide. *J. Am. Chem. Soc.* **2015**, *137*, 8696−8699.
(25) Zhou, H.; Chen, Q.; Li, G.; Luo, S.; Song, T. b.; Duan, H. S.; Hong, Z.; You, J.; Liu, Y.; Yang, Y. Interface Engineering of Highly Efficient Perovskite Solar Cells. *Science* **2014**, *345*, 542−546.
(26) Snaith, H. J.; Grätzel, M. Enhanced Charge Mobility in a Molecular Hole Transporter via Addition of Redox Inactive Ionic Dopant: Implication to Dye-Sensitized Solar Cells. *Appl. Phys. Lett.* **2006**, *89*, 262114.
(27) Burschka, J.; Dualeh, A.; Kessler, F.; Baranoff, E.; Cevey-Ha, N.-L.; Yi, C.; Nazeeruddin, M. K.; Grätzel, M. Tris(2-(1H-pyrazol-1-yl)pyridine)cobalt(III) as p-Type Dopant for Organic Semiconductors and Its Application in Highly Efficient Solid-State Dye-Sensitized Solar Cells. *J. Am. Chem. Soc.* **2011**, *133*, 18042−18045.
(28) Furube, A.; Katoh, R.; Hara, K.; Sato, T.; Murata, S.; Arakawa, H.; Tachiya, M. Lithium Ion Effect on Electron Injection from a Photoexcited Coumarin Derivative into a TiO_2 Nanocrystalline Film Investigated by Visible-to-IR Ultrafast Spectroscopy. *J. Phys. Chem. B* **2005**, *109*, 16406−16414.
(29) Cappel, U. B.; Smeigh, A. L.; Plogmaker, S.; Johansson, E. M. J.; Rensmo, H.; Hammarström, L.; Hagfeldt, A.; Boschloo, G. Characterization of the Interface Properties and Processes in Solid State Dye-Sensitized Solar Cells Employing a Perylene Sensitizer. *J. Phys. Chem. C* **2011**, *115*, 4345−4358.
(30) Abate, A.; Leijtens, T.; Pathak, S.; Teuscher, J.; Avolio, R.; Errico, M. E.; Kirkpatrik, J.; Ball, J. M.; Docampo, P.; McPherson, I.; Snaith, H. J. Lithium Salts as "Redox Active" p-Type Dopants for Organic Semiconductors and Their Impact in Solid-State Dye-Sensitized Solar Cells. *Phys. Chem. Chem. Phys.* **2013**, *15*, 2572−2579.
(31) Bai, Y.; Zhang, J.; Wang, Y.; Zhang, M.; Wang, P. Lithium-Modulated Conduction Band Edge Shifts and Charge-Transfer Dynamics in Dye-Sensitized Solar Cells Based on a Dicyanamide Ionic Liquid. *Langmuir* **2011**, *27*, 4749−4755.
(32) Krüger, J.; Plass, R.; Cevey, L.; Piccirelli, M.; Grätzel, M.; Bach, U. High efficiency solid-state photovoltaic device due to inhibition of interface charge recombination. *Appl. Phys. Lett.* **2001**, *79*, 2085−2087.
(33) Cappel, U. B.; Daeneke, T.; Bach, U. Oxygen-Induced Doping of Spiro-MeOTAD in Solid-State Dye-Sensitized Solar Cells and Its Impact on Device Performance. *Nano Lett.* **2012**, *12*, 4925−4931.
(34) Yang, L.; Xu, B.; Bi, D.; Tian, H.; Boschloo, G.; Sun, L.; Hagfeldt, A.; Johansson, E. M. J. Initial Light Soaking Treatment Enables Hole Transport Material to Outperform Spiro-OMeTAD in Solid-State Dye-Sensitized Solar Cells. *J. Am. Chem. Soc.* **2013**, *135*, 7378−7385.
(35) Abate, A.; Hollman, D. J.; Teuscher, J.; Pathak, S.; Avolio, R.; D'Errico, G.; Vitiello, G.; Fantacci, S.; Snaith, H. J. Protic Ionic Liquids as p-Dopant for Organic Hole Transporting Materials and Their Application in High Efficiency Hybrid Solar Cells. *J. Am. Chem. Soc.* **2013**, *135*, 13538−13548.
(36) Li, Z.; Tinkham, J.; Schulz, P.; Yang, M. J.; Kim, D. H.; Berry, J.; Sellinger, A.; Zhu, K. Acid Additives Enhancing the Conductivity of Spiro-OMeTAD Toward High-Efficiency and Hysteresis-Less Planar Perovskite Solar Cells. *Adv. Energy Mater.* **2017**, *7*, 10.1002/aenm.201601451.
(37) Han, C. C.; Elsenbaumer, R. L. Protonic Acids: Generally Applicable Dopants for Conducting Polymers. *Synth. Met.* **1989**, *30*, 123−131.
(38) dos Santos, D. A.; Galvão, D. S.; Laks, B. Protonic Doping Effects on the Electronic Behavior of Poly(p-phenylene-co-2,5-pyrazine). *Solid State Commun.* **1990**, *74*, 215−217.
(39) Spangler, C. W.; Bryson, P.; Liu, P.-K.; Dalton, L. R. Protonic Doping of Bis-thienylpolyenes and Oligomers of Poly (2,5-thienylenevinylene): Comparison to Oxidative Chemical Doping. *J. Chem. Soc., Chem. Commun.* **1992**, 253−254.
(40) Hu, B.; Zhu, X.; Chen, X.; Pan, L.; Peng, S.; Wu, Y.; Shang, J.; Liu, G.; Yan, Q.; Li, R. W. A Multilevel Memory Based on Proton-Doped Polyazomethine with an Excellent Uniformity in Resistive Switching. *J. Am. Chem. Soc.* **2012**, *134*, 17408−17411.
(41) Margaretta, E.; Olmeda, C.; Yu, L. Doped Polyaniline in Brønsted Acid Ionic Liquid 1-butyl-3-methylimidazolium bis-[trifluoromethyl(sulfonyl)]imide/ bis[trifluoromethyl(sulfonyl)]imide. *J. Appl. Polym. Sci.* **2013**, *127*, 2453−2457.
(42) Li, L.-L.; Chang, Y.-C.; Wu, H.-P.; Diau, E. W.-G. Characterisation of electron transport and charge recombination using temporally resolved and frequency- domain techniques for dye-sensitised solar cells. *Int. Rev. Phys. Chem.* **2012**, *31*, 420−467.
(43) Xu, M.; Rong, Y.; Ku, Z.; Mei, A.; Li, X.; Han, H. Improvement in Solid-State Dye Sensitized Solar Cells by p-Type Doping with Lewis Acid $SnCl_4$. *J. Phys. Chem. C* **2013**, *117*, 22492−22496.
(44) Itzhaik, Y.; Bendikov, T.; Hines, D.; Kamat, P. V.; Cohen, H.; Hodes, G. Band Diagram and Effects of the KSCN Treatment in TiO_2/Sb_2S3/CuSCN ETA Cells. *J. Phys. Chem. C* **2016**, *120*, 31−41.
(45) Kopidakis, N.; Benkstein, K. D.; van de Lagemaat, J.; Frank, A. J. Transport-Limited Recombination of Photocarriers in Dye-Sensitized Nanocrystalline TiO_2 Solar Cells. *J. Phys. Chem. B* **2003**, *107*, 11307−11315.
(46) Bai, Y.; Zhang, J.; Wang, Y.; Zhang, M.; Wang, P. Lithium-Modulated Conduction Band Edge Shifts and Charge-Transfer Dynamics in Dye-Sensitized Solar Cells Based on a Dicyanamide Ionic Liquid. *Langmuir* **2011**, *27*, 4749−4755.
(47) Kelly, C. A.; Farzad, F.; Thompson, D. W.; Stipkala, J. M.; Meyer, G. J. Cation-Controlled Interfacial Charge Injection in Sensitized Nanocrystalline TiO_2. *Langmuir* **1999**, *15*, 7047−7054.
(48) Daeneke, T.; Mozer, A. J.; Kwon, T. H.; Duffy, N. W.; Holmes, A. B.; Bach, U.; Spiccia, L. Dye Regeneration and Charge Recombination in Dye-Sensitized Solar Cells with Ferrocene Derivatives as Redox Mediators. *Energy Environ. Sci.* **2012**, *5*, 7090−7099.
(49) van de Krol, R.; Goossens, A.; Meulenkamp, E. A. Electrical and Optical Properties of TiO_2 in Accumulation and of Lithium Titanate $Li_{0.5}TiO_2$. *J. Appl. Phys.* **2001**, *90*, 2235−2242.

DOI: 10.1021/acs.jpcc.7b07958
J. Phys. Chem. C 2017, 121, 18472−18479